Intelligent Carpet System, Based on Photonic Guided-Path Tomography, for Gait and Balance Monitoring in Home Environments

Jose A. Cantoral-Ceballos, *Member, IEEE*, Nurgiyatna Nurgiyatna, Paul Wright, John Vaughan, Christine Brown-Wilson, Patricia J. Scully, and Krikor B. Ozanyan, *Senior Member, IEEE*

***Abstract*— We report on the photonic variant of the previously introduced guided-path tomography (GPT), by demonstrating a system for footstep imaging using plastic optical fiber (POF) sensors. The 1 m × 2 m sensor head is manufactured by attaching 80 POF sensors on a standard commercial carpet underlay. The sensing principle relies on the sensitivity of POF to bending, quantified by measuring light transmission. The photonic GPT system, comprising the sensor head with processing hardware and software, covered by a mass-production general-purpose carpet top, successfully performs footstep imaging and correctly displays the position and footfall of a person walking on the carpet in real time. We also present the implementation of fast footprint center of mass calculations, suitable for recording gait and footfall. A split-screen movie, showing the frame-by-frame camera-captured action next to the reproduced footprints, can be downloaded at http://ieeexplore.ieee.org**

***Index Terms*— Footstep imaging, gait, "intelligent carpet," parallel center of mass algorithm (PCoMA), photonic guided-path tomography (PGPT), plastic optical fiber (POF).**

Manuscript received May 1, 2014; accepted June 26, 2014. Date of publication July 20, 2014; date of current version November 6, 2014. This work was supported by the Engineering and Physical Sciences Research Council of the U.K., through the Knowledge Transfer and other schemes. The associate editor coordinating the review of this paper and approving it for publication was Dr. Ravinder S. Dahiya.

J. A. Cantoral-Ceballos, N. Nurgiyatna, P. Wright, and K. B. Ozanyan are with the School of Electrical and Electronic Engineering, Faculty of Engineering and Physical Sciences, University of Manchester, Manchester M13 9PL, U.K. (e-mail: jose.cantoralceballos@manchester.ac.uk; nungnurgie@gmail.com; p.wright-2@manchester.ac.uk; k.ozanyan@manchester.ac.uk).

J. Vaughan and P. J. Scully are with the School of Chemical Engineering and Analytical Science, Faculty of Engineering and Physical Sciences, University of Manchester, Manchester M13 9PL, U.K., and also with the Photon Science Institute, University of Manchester, Manchester M13 9PL, U.K. (e-mail: j.vaughan@manchester.ac.uk; patricia.scully@manchester.ac.uk).

C. Brown-Wilson is with the School of Nursing, Midwifery and Social Work, Faculty of Medicine and Health Sciences, University of Manchester, Manchester M13 9PL, U.K. (e-mail: christine.brownwilson@manchester.ac.uk).

This paper has supplementary downloadable multimedia material available at http://ieeexplore.ieee.org provided by the authors. The Supplementary Material is a split-screen video showing, on the left side, a person walking on the "Intelligent carpet" and, on the right, the real-time iterative Landweber reconstruction of the person's footprint. The file is a video in Audio Video Interleave (.AVI) format. This material is 5.80 MB in size.

Color versions of one or more of the figures in this paper are available online at http://ieeexplore.ieee.org.

Digital Object Identifier 10.1109/JSEN.2014.2341455

I. Introduction

In THIS work, 'intelligent carpet' is defined as an ordinary carpet supported by a sensor system capable of capturing, processing and presenting information on human footsteps. Generally, this task can be achieved by systems of varying complexity, portability and cost, depending on the context in which they are deployed. A number of methods for footstep sensing have been proposed and developed since the 1980s, involving piezoelectric [1], [2], resistive [3], force [4], [5], capacitive [6], seismic [7] and acoustic sensing principles [8]. The utilized sensing technology has included load cells [9], [10], switches [11], electromechanical films [12], optical fibers [13], flatbed scanners [14], resistive loads [15] and accelerometers [16], as well as combinations thereof [17]. The terminology used has varied depending on the application, e.g. "magic" carpet [2], floor sensor [3], active floor [4], pressure sensing floor [5], smart carpet [6] and smart floor [9].

This work uses a tomographic method, based on Guided-Path Tomography (GPT) [18], to image the deformation induced by the footfall. GPT is suitable for covering substantial areas involving measurements at their periphery only, reducing the number of measurements and sensor connections per unit area. Thus simple, portable and affordable GPT systems have the potential to span across the healthcare, sports, entertainment, security and other sectors, where the floor contact of one or more individuals can be recorded and analyzed in a non-intrusive way.

In this introduction, we present gait analysis as one of the system's possible targets. Gait recognition based on GPT could lead to applications exploiting information of biometric character, such as asymmetry (limping), variability (unsteadiness), compensatory strategies and adaptive gait. Gait, as a walking pattern, comprises the speed of walking, the distance between footsteps (in longitudinal and lateral direction) and the pattern of the footfall. To date, data for gait recognition have been collected typically by three different methods based on video sensing, floor sensors or wearable sensors. In addition to cost, these options also vary in their intrusiveness resulting in privacy concerns, as well as dependence on the subject's cooperation. Being a floor sensor, the reported GPT system does not interfere with the subject's daily environment allowing unperturbed behavior, as contrasted with attaching wearable devices to their body,

or possible ethical concerns from being constantly monitored by video cameras [19]. Furthermore, the GPT system works on deformation caused by gravity acting on the person's body mass, which cannot be eliminated or compromised, and therefore ensures the necessary degree of cooperation by the subjects involved. As opposed to other floor sensors, the GPT "intelligent carpet" images deformation, which integrates a number of additional indicators of gait and balance related to medical conditions, such as the position of the body mass center, joint mobility, symmetry and plantar pressure.

Our reported demonstrator is an "intelligent carpet" based on photonic GPT (PGPT) with 80 POF sensors. It covers an area of 1 m $\times$ 2 m with a spatial resolution of 0.06 m and is capable of displaying the image of footsteps in real time, as well as storing the measurement data for further processing and analysis. The two main parameters of the system, the spatial and temporal resolution, are not independent and are individually determined by the number and positioning of the POF sensor elements, the mechanical properties of the substrate material, as well as the performance of the acquisition and processing electronics combined with the speed of the data processing algorithms.

The rest of the paper is organized as follows: Section II reviews other systems based on floor sensors. Section III examines the details concerning the POF sensor elements. Section IV elucidates PGPT, the imaging principle employed by the system. Section V presents the details of the imaging mat demonstrator and Section VI shows the obtained results. Section VII offers a brief discussion and concludes the paper. This paper is expanded from conference papers presented at IEEE Sensors 2010 [20] and at IEEE Africon 2011 [21].

II. Background

It has been reported that in a normal state, the walk period of an average human is typically 1.2 s, which is double to duration of a single step full cycle [22]. Within this step period of 0.6 s, the touchdown time of the foot is around 0.2 s. Considering the duration of the gait events, the time resolution or image frame rate of the system required for simple gait recognition has to be at least 10 Hz (100 ms imaging period).

In terms of spatial resolution, the distance between the metatarsus and calcaneus bones varies depending on each individual. The average arch length of the adult foot, measured from the back of the heel to the metatarsal bone, has been reported to be 0.189 m [23] (from a sample of 100, including both male and female individuals). Based on this result, the expected separation between the calcaneus and metatarsal bones is approximately 0.15 m. Therefore, any system used for identifying the position of these points of pressure must be able to resolve at least this distance.

In one of the early implementations, a piezoelectric cable was used to build a floor sensor system of size 3.0 m $\times$ 1.8 m [2]. The system, called 'the magic carpet', had an approximate scan rate of 60 Hz with spatial resolution of approximately 0.1 m. This has been successfully implemented to monitor dynamic foot position and pressure for an interactive musical application; however its utility for gait analysis is unknown.

A 2.4 m $\times$ 2.0 m system, based on capacitive sensors, was demonstrated by embedding electronics in textiles and interleaving them inside a carpet [6]. It was capable of tracking the path of a walker with an estimated 98% accuracy; however its suitability for gait analysis is unclear.

Footstep recognition in a "smart home" was addressed in [24]. Here two piezoelectric transducers were inserted into the underside of a rubber floor tile and used to collect data of 3,550 footsteps from 55 subjects. Although the system was implemented for footstep recognition, it can only capture footstep signals at a strictly defined permanent location. Subsequent work by the same authors employed two sensor mats of 0.45 m $\times$ 0.35 m, each containing 88 piezoelectric sensors [25], capable of capturing two consecutive footstep signals. It should be noted that the work addressed in that research aims at generating a footstep database for biometric identification and hence, it requires special laboratory facilities using video cameras and microphones.

A distributed sensing floor, based on fiber optics, employed 40 m of meandering fiber to cover an area of 1.6 m $\times$ 4.0 m [13]. Brillouin Optical Time-Domain Analysis (BOCDA) was applied to locate the strain deviation along the fiber in 3.6 s. A special processing algorithm was implemented allowing a tracking speed of 1.7 m/s. The system was intended for personnel presence detection only and the tracking was with spatial resolution of 0.18 m. In addition, the use of BOCDA requires a signal generator, laser and frequency modulator which increase the complexity of the system and substantially raises its cost, limiting its applications outside the laboratory environment.

An electronic walkway has been made commercially available under the brand name GAITRite System [26]. It consists of sensor pads, each containing 2304 sensors arranged in a 48 $\times$ 48 grid, typically covering a total active area of 1 m $\times$ 6 m. It is capable of measuring spatial and temporal gait parameters and is portable. The GAITRite has been used by physiotherapists as part of clinical assessment, but its cost is substantial. This limits its usage to a laboratory tool rather than an affordable system potentially deployable in new homes or retro-fitted in existing dwellings.

Within the variety of sensing methods employed, most of the implementations are based on the same principle, which is utilizing the force exerted on the sensing device as a result of the mass of the subject and its impact on the device. The latter is related to the Ground Reaction Force (GRF), defined as the reaction of the device in response to the weight and inertia of an object [9]. The resultant GRF per unit contact area yields the pressure exerted. The coordinates of the point, where the resultant of all ground reaction forces acts, are defined as the "Centre of Pressure" (CoP) coordinates. The CoP changes in time depending on balance and gait.

The sensing principle used in this work is also a type of a GRF sensing and in that sense offers advantages over binary sensor arrays [2], [6], [26]. It employs Plastic Optical Fibers (POFs) sensitive to how their underlying substrate deforms as a result of the pressure exerted on the carpet surface. The deformation magnitude depends on the weight of the subject under test (SUT) and the mechanical properties of the

TABLE I
SUMMARY OF REVIEWED FLOOR SYSTEMS

System	Size [m x m]	Spatial res.[m]	Temporal res. [Hz]
'The magic carpet' [2]	3.00 x 1.80	0.10	~ 60
Textile-embedded electronics [6]	2.40 x 2.00	0.05*	NA
'Smart Home' [22]	0.45 x 0.35	NA	NA
BOCDA [13]	1.60 x 4.00	0.18	~ 0.44
GAITRite [23]	1.00 x 6.00	0.0127	Up to 240
'Intelligent Carpet'	**1.00 x 2.00**	**0.06†**	**>60‡**

*only on sensing areas
†from distance between path integrals
‡without sample averaging
NA = Not Available

underlay that separates the POF sensor from un-deformable ground. The POF sensor utilizes light intensity transmission measurements and compared to other sensing methods offers the advantages of ruggedness, intrinsic safety and resistance to body fluids such as blood and urine. Typically, POF is available at the cost of less than 1 USD/m and can be combined with inexpensive, light and miniature optoelectronic light sources and detectors for the manufacture of energy-efficient sensor elements. Furthermore, it is straightforward to integrate the POF sensor elements with a standard commercial underlay commonly used for carpeting, allowing the sensor head to remain inconspicuous under the normal carpet surface in the daily living space.

In view of the studies presented thus far, it is possible to conclude that although the studied systems meet the spatial and temporal resolution requirements for monitoring of gait and walking habits, they are suitable mainly for laboratory use and/or interfere with personal privacy. They also come at a considerable cost, which limits their potential deployment on large floor areas. The cost of materials for manufacturing the "intelligent carpet" sensor head is below 150 USD/sq.m. A comparison of the spatial and temporal resolution achieved by each system is given in Table I, where the last row (in bold) represents this work.

III. PLASTIC OPTICAL FIBER SENSORS FOR PGPT

Sensing elements based on deformation or bending exerted on optical fibers have been used in measuring systems for monitoring pressure, strain, vibration, displacement, velocity, acceleration [27]. In such applications POFs are a more natural choice, because of their higher sensitivity to bending compared to glass fibers. However, the POF sensitivity to bending is still weak in absolute values. To account for this limitation, several authors have demonstrated methods to enhance their sensitivity by embedding an imperfection in the fiber, which modulates its wave-guiding properties as a function of the bending radius [28]–[33]. In [28], a fiber optic strain gauge was developed by inserting radial grooves into a multimode plastic optical fiber to increase curvature measurement sensitivity. In [29], a segment of the POF cross-sectional profile was removed over a predetermined length to improve the strain sensitivity by abrading the POF surface with a razor blade. In [30], a sensitive zone was produced by physical treatment

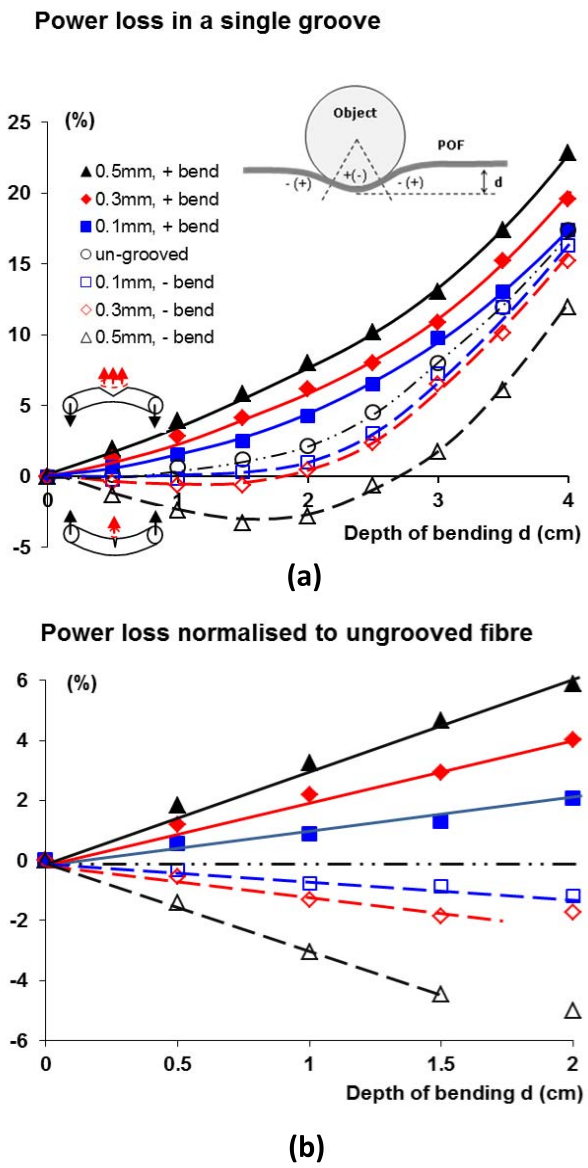

Fig. 1. (a) Dependence of the power loss in a single groove on the depth of bending for different groove depths. (b) Same plots, but with the contribution from the un-grooved fiber subtracted. The insets illustrate positive (opening of grooves) or negative (closing of grooves) bending (with signs in brackets denoting grooves oriented towards the object), as well as the depth of bending d [20]. The lines are guides to the eye only.

(milling, grinding) with a light emission (loss) surface along one side of the fiber only.

By far the simplest and least expensive way to enhance the POF sensitivity to bending is to manufacture grooves of suitable depth and period along the POF length. It has been shown by ray-tracing, simulations and measurements [34], [35] that, in general, grooved POF sensitivity arises from the 'opening' or 'closing' of the groove resulting from positive or negative bending respectively [34]–[37]. Most of the calculations and experimental evaluations have been concerned with a set of comparatively shallow groove structures.

Compared to existing literature, we have measured the power loss in a single groove of larger depths, from 0.1 mm to 0.5 mm, the latter being comparable with the POF radius.

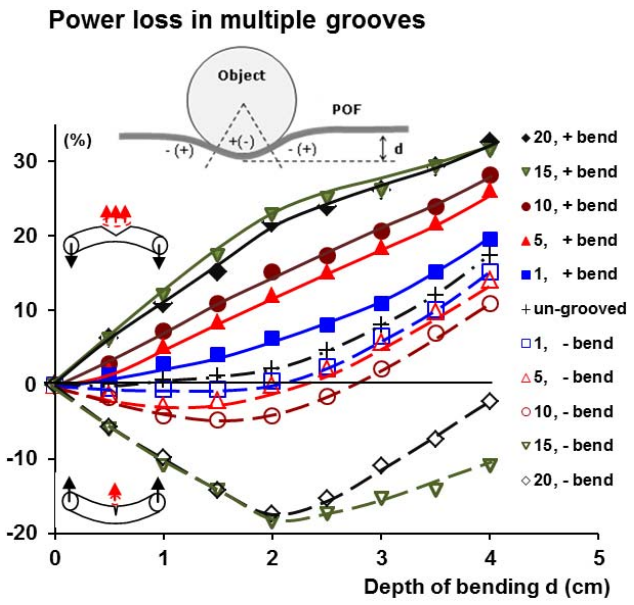

Fig. 2. Power loss contribution from a varying number of multiple grooves, cut to different depths. The inset shows that both positive and negative bending take place. Signs refer to grooves facing away from the object (in brackets - facing the object) for a certain degree of deformation, resulting in decrease in sensitivity. The depth of bending d is defined in [20]. The lines are a guide to the eye only.

This was motivated by the particular application requiring sensitivity to human footprints on commercially available combinations of carpet and underlay. Fig. 1 summarizes the characteristic response of some of our POF sensors to bending by a cylinder of radius 3.75 cm, driven to deform a soft foam substrate onto which the grooved POF is firmly attached. The POF (PGR-FB1000, Toray Industries, Inc.) of diameter 1 mm was step-index, with a 0.98 mm core of high-purity poly-methyl-methacrylate and cladding of special fluorinated polymer. Positive or negative bending was achieved by the groove facing away or towards the deforming cylinder, respectively. Further experimental details are given in [20].

The results in Fig. 1 show that relative gain (negative loss) in the transmitted power is observed consistently when the grooves are facing the deforming cylinder (negative bending). The contribution by the groove is reasonably linear for groove depths up to half the radius of the deforming cylinder. The relative gain experiences a maximum depending on the groove depth. At large bending depths the behavior is similar to that of an un-grooved POF and careful calibration is necessary for operation in that range.

Fig. 2 shows measurement results obtained under similar conditions on a group of equidistant grooves (in some experiments up to 30, while keeping the grooves' separation the same for any number of grooves), thus the overall sensitized length being directly proportional to the number of grooves. In this case, since the POF is attached to the deforming substrate, it is possible to distinguish three adjacent sections of the POF, as shown in the inset of Fig. 2: the bending changes sign upon transition to the neighboring section. This impacts on the dependence of the losses from the depth of bending. Indeed, while the sensitivity increases with the depth up to about 2 cm, similar to the single groove case, further deformation results in decrease in sensitivity, since the transmitted signal now as well integrates the contribution from sections with the opposite bending sign. This is also corroborated by the decrease in sensitivity being manifested stronger at a larger number of grooves, apparently due to the larger overall sensitized length, to include all three adjacent sections as per the inset of Fig. 2.

TABLE II
MECHANICAL INTEGRITY OF GROOVED POF AT REPETITIVE BENDING

Bending shape	Groove depth (mm)	d1 (cm)	d2 (cm)	Number of cycles
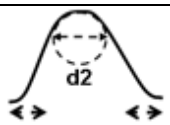	0.5	-	3	1480
	0.1	-	3	3480
	0.5	-	4	13400
	0.1	-	4	35000
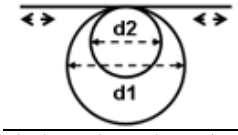	0.5	9	5	34920
	0.5	10	6	183600
	0.5	11	7	>250000

The last column shows the average number of repetitive bends at which the POF breaks

For the design of a POF sensor with embedded imperfections, it is essential to clarify to what extent the mechanical integrity is compromised by these imperfections, since the POF should accommodate repeated exposure to bending. This is even more imperative in the case of grooving, since the manufacture of grooves can cause micro-cracks or other defects in the POF material. To address this problem, we performed repetitive bending tests on single- and multiple-groove POFs, in order to observe the conditions for breakage. In all experiments, one end of the grooved POF was fixed, while the other was displaced along a straight line by end of a metal arm oscillating with up to 1000 cycles/minute. Table II presents results in the critical zone, where POF breakages have been observed, except for the last row where the mechanical integrity has not been breached even after 2.5×10^5 events of bending down to a radius of 3.5 cm. Table II is structured according to the type of bending experiment (bell-shaped geometry for smaller bending radii and loop geometry for larger bending radii) and groove depth. It is important to note here that we have compared groove depths of 0.1 mm and 0.5 mm, the former being the typical upper limit of groove depth used in literature and the latter reaching the extreme upper limit for the groove depth in POF of $\sim$1 mm in diameter. At small bending radii, the suggested impact of micro-cracks and other defects generated by the groove manufacture is corroborated by the observation that decreasing the groove depth from 50% to 10% of the POF diameter improves the breakage time by a factor of $\sim$23 times. It should be noted that in our intended application, events of severe bending will occur at a frequency much lower than the oscillation frequency above. This suggests that, depending on the POF material properties, the useful lifetime of the sensor will exceed substantially the above estimates. Indeed, the bending radii in the bell-shaped geometry and the groove depth in the loop-shaped geometry are outside the range of realistic conditions and design rules.

Generally, the results indicate that un-grooved POFs already have inherent sensitivity to bending typical for this application; however, grooving the POF enhances that sensitivity. In realistic experiments, with an average person standing on a single bare foot on a carpet with a POF, the power loss in un-grooved POF was 1.48 ± 0.01% while that for POF with 25 grooves separated by 1cm is 7.64 ± 0.17%. The measured signals will also depend on the mechanical properties of the substrate, as the bending of the POF replicates the deformation of the top surface and underlay. Therefore, the details in the choice of technology for an "intelligent carpet" system will depend on the particular details of construction and deployment.

IV. Photonic Guided-Path Tomography

At first sight, applying tomography for imaging of deformation is self-contradictory because usually tomography is associated with either strictly in-plane imaging (e.g. in early x-ray tomography systems) or with elaborate 3D imaging of subjects with substantial out-of-plane spatial distribution (e.g. electrical tomography) [38]. However, GPT allows imaging in non-planar surfaces determined by the guided paths.

GPT has been introduced and demonstrated for temperature imaging [18], where the line-integrals, traditionally of (weak) x-ray attenuation across the subject

$$\Phi \approx \Phi_0 \int_0^L \mu(l) dl, \tag{1}$$

($\mu(l)$ – attenuation coefficient along the beam; $\Phi-$ photon flux, L – distance from source to detector), are replaced by path-integrals of resistivity along metal wires

$$R = \frac{1}{A} \int_0^L \rho(T(l)) dl, \tag{2}$$

($\rho(l)$ - resistivity along the wire; R - wire resistance), which can deviate from strict 2D planarity. In the photonic implementation of GPT (PGPT), instead of wires we use optical fiber transducers [39]; therefore (1) and (2) have their equivalent in PGPT as

$$\phi = \phi_0 \int_0^L a(D(x, y, z)) dl, \tag{3}$$

where a stands for the apparent attenuation coefficient (AAC) along the fiber, D is the deformation field and the transmittance through the fiber is given by φ/φ_0, which is the quantity of interest in the case of POF bending in Section III. Thus we have an example of different physical phenomena described by similar expressions (1)-(3). The relevance of applying the established theory and practice of inverting the Radon transform [38], [40] for PGPT has been addressed earlier [41], [42], demonstrating the validity of the assumptions for an exponential Beer-Lambert attenuation, as well as the impact of the losses incurred being independent from their position along the POF element. Furthermore, the measurements quoted the last paragraph in Section III show that the integrated loss along the POF can be kept low to justify taking a linear expression in (3) instead of exponential.

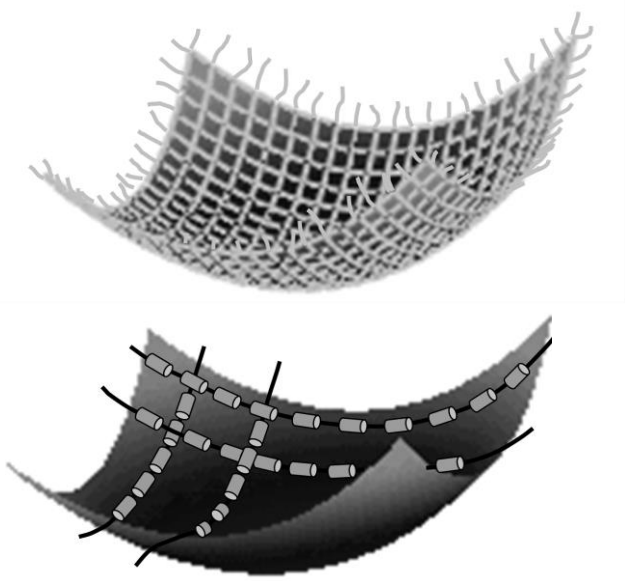

Fig. 3. Artist's impression of an "intelligent carpet" sensor head, comprising of un grooved POF transducers (top) and grooved POF transducers (bottom), providing path integrals of attenuation due to bending. The simplest possible case of only two perpendicular views is shown. Repetitive sections with one or more groves are depicted as discrete cylinders along the length of the POF transducer.

An essential factor for the choice of PGPT, as the base for developing an "intelligent carpet" sensor head and system, is that the POF elements introduce characteristics typical of a distributed sensor and is particularly efficient for large areas. Indeed, PGPT allows a saving of N×(N-2) measurements and N×(2N-4) contact wires over an N×N array of single-point sensors with two contact wires [18]. Additionally, the deployment of single-point sensors is inefficient even for moderately large areas, since for reasons of access, cost, etc. the achievable spatial sampling rate is typically much lower than the spatial precision of the measurement.

The cases of un-grooved and grooved POF sensors present obvious embodiments of continuous and discrete transducers, as introduced in GPT [18]. Fig. 3 shows an impression of the "intelligent carpet" incorporating such transducers, in the discrete case connected in series, to allow path integral measurements. The grooved POF case implies that contributions from both un-grooved and grooved sections may be substantial because the later are connected by un-grooved POF, which is also required for connecting to the light source and detector. Thus, for any POF transducer, (3) can be expressed in terms of power loss as

$$\frac{\phi}{\phi_0} = \left\{ \int_U a\left(D\left(l\right)\right) dl + \sum_G a_G l_G \right\} + \phi_C, \tag{4}$$

here the integration is over all of the un-grooved sections of the POF (which may not be adjacent) and the summation is over all of the grooved sections containing one or more grooves; a is the AAC and a_G stands for the average AAC for a grooved section of length l_G. Since some bending on

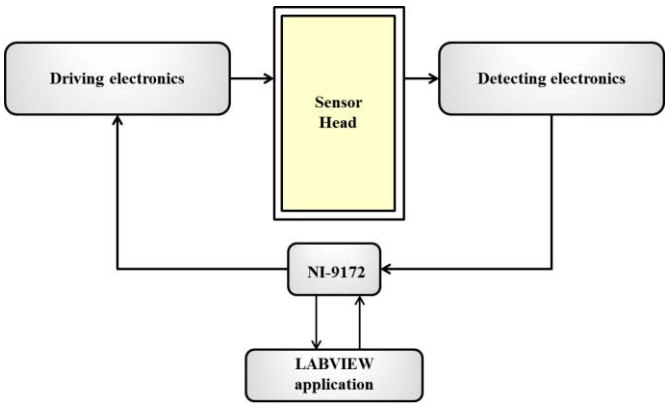

Fig. 4. Block diagram of the intelligent carpet system.

the POF transducer is inevitable, even without a deforming load, an initial power loss calibration measurement ϕ_C is required from all POF transducers in the absence of the SUT; then the forward Radon transform is defined as the set of measurements given by the bracketed term in (4) for each POF, representing the signal differences between the calibration and the actual measurements. This approach also allows, at the imaging stage, to exclude all static objects on the carpet (such as furniture) reconstructing only the dynamic footprint images by data inversion, in addition it accounts for any residual deformation present in the mat.

Some pilot PGPT results with light (2 to 5 kg) household objects on a 0.8 m $\times$ 0.8 m PGPT imaging mat have been presented earlier [21]; however that pilot was not suitable for real-time footprint imaging. Based on the combination of the background given in Section III with the PGPT concept presented throughout this Section, we integrated a complete "intelligent carpet" system capable of mapping in real time the deformation induced by an average-weight person walking on it. The following section presents a larger demonstrator in the form of an intelligent carpet with a sensor head consisting of a combination of a commercially available carpet top and a PGPT-enabled commercial carpet underlay.

V. "Intelligent Carpet" Demonstrator

The PGPT system developed is an integration of three parts: sensor head, driving and detecting electronics and processing/imaging unit (see Fig. 4), which are explained below.

A. Sensor Head

As already outlined in the end of Section IV, the sensor head incorporates an active PGPT layer made of a number of POFs that are strategically placed and firmly attached (using water-based synthetic latex flooring adhesive) onto a rectangular carpet underlay to allow the required spatial resolution. The underlay and PGPT layer are then covered by a standard pile carpet (see Fig. 5) that matches the dimensions of the underlay, resulting in an intelligent carpet system of imaging area of 1.0 m $\times$ 2.0 m. Pencil-beam type path integrals are utilized as sampling geometry in the PGPT layer and several adjacent modules of underlay with a POF layer can be covered by a continuous top carpet layer to form a larger imaging area of different shapes. The main challenge in the design of the sensor head is to match the number and position of the POF transducers to the required spatial resolution and imaging frame rate, as well as cost. In the setup presented, 80 POF sensors were distributed (unevenly) across three projections at 0 (14 beams), 60 and 120 degrees (with 33 beams each), with a constant separation of 0.06 m, as shown in Fig. 6.

Fig. 5. A cut-out of the sensor head showing the cross section with the top pile carpet, the position of the POF layer and the underlay.

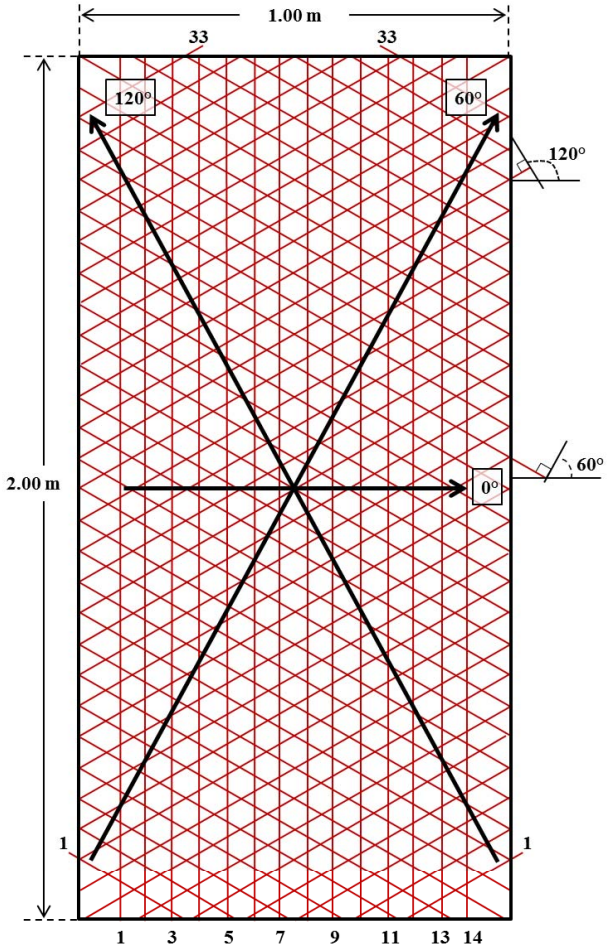

View @ 0°		View @ 60° and @ 120°	
# beams	*Δs (m)*	# Beams	*Δs (m)*
14	0.06	33	0.06

Fig. 6. Diagram with geometry used in sensor head.

B. Driving and Detecting Electronics

Light emitting diodes (LEDs) are coupled at one end of the POF to launch light. At the other end, each POF is coupled to a separate photodiode to measure light intensity, enabling parallel acquisition of independent transducer measurements. This is in contrast to our previously reported pilot implementations where light was launched by individual LEDs and all POFs were bundled and butt-coupled to a single large-area photodiode [20]. Since the principle for sampling the forward Radon transform is to have the path integral measurements taken independently, using a single source and individual detectors is an alternative. However, for the typical number of POF transducers used in the demonstrator, the preferred choice is to use individual sources and detectors, multiplexed to a single output for serial acquisition. This is dictated by the optimum balance between complexity, performance and cost, still allowing the data rates required for real-time imaging of footsteps. All launch and receive devices (80 pairs) and their connections are fitted within a frame (flush with the carpet) at the periphery of the sensor head, together with the electronics control unit, based on a Programmable Logic Device (PLD).

The acquired signals are interfaced to an external laptop via a LabVIEW environment using a NI-9205 analog input module connected through a NI-cDAQ-9172 chassis. Although the upper limit for driving the 80 LEDs sequence and acquisition exceeds 60 Hz, in the results presented further this is capped to match the speed of real-time imaging. This allows to implement considerable bandwidth narrowing for improved signal-to-noise, achieved by the averaging of 250 measurement samples. Under these circumstances, the data scan of the complete frame takes 328 ms, corresponding to ∼3 frames/s (fps). This cap on the speed is not firm and depends on the external computer hardware used for image reconstruction. Most certainly, such a limit can be removed with hardware acceleration.

C. Imaging

The data acquired from the sensor head constitute a severely under-sampled Radon transform, because the system design envelope allows only an extremely small number of angular projections containing a fairly low number of individual path integrals. Under these conditions, the starting point for real-time imaging of the deformation from footsteps is implemented by using the iterative Landweber method (ILM) [42]–[44] with median filtering of the data at each iteration. This method has been shown to achieve satisfactory reconstructions from as little as 28 line integrals in near-IR absorption tomography of fuel in internal combustion engines [45]. The image reconstruction algorithm was developed in MATLAB for testing and then transported to LabVIEW for reconstruction from real-time data.

We have shown previously the potential of applying sinusoidal Hough transform, followed by peak thresholding on severely under-sampled sinograms (i.e. image representations of the Radon transform) [46]. In addition to sinogram recovery for further applying the inverse Radon transform, this approach allows fast and computationally efficient "center-of-mass"

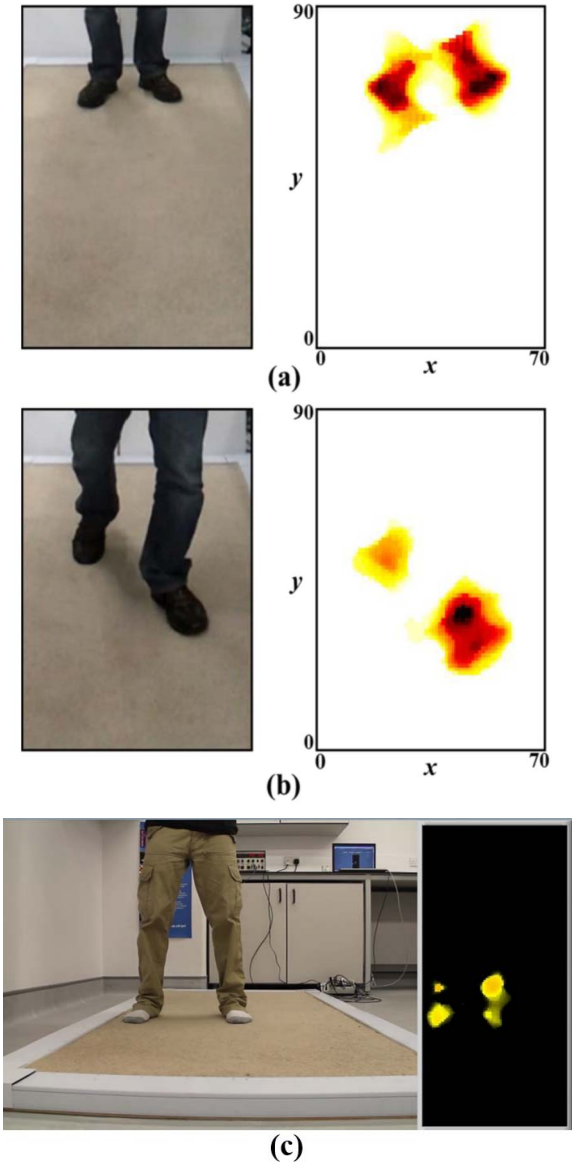

Fig. 7. Imaging results from a standing position (a) and walking (b), (c), using the iterative Landweber method (ILM). (c) Shows the deformation when standing with bare feet.

reconstruction [47] suitable for applications where the dynamics of the SUT is of greater interest than its internal distribution and the details of its contours. In hardware implementations, the utilization of the Parallel Center-of- Mass Algorithm (PCoMA) [21], [48][1] allows a drastic reduction of the time for data inversion, down to microseconds, independent of the number of SUTs in the imaging frame.

It is important to note here that the CoM methods, including PCoMA, deliver the CoM coordinates without reconstructing the whole image. In PCoMA, the centers of attenuation "mass" in each angular projection are used to reconstruct the geometric center of a two-dimensional cross-section of the SUT. In the context of gait analysis with an "intelligent

[1]In this context, "Centre-of Mass" concerns the "mass" of a single tomographic projection (see [45]–[47]), not to be confused with terminology related to the mass of a human body in gait analyses.

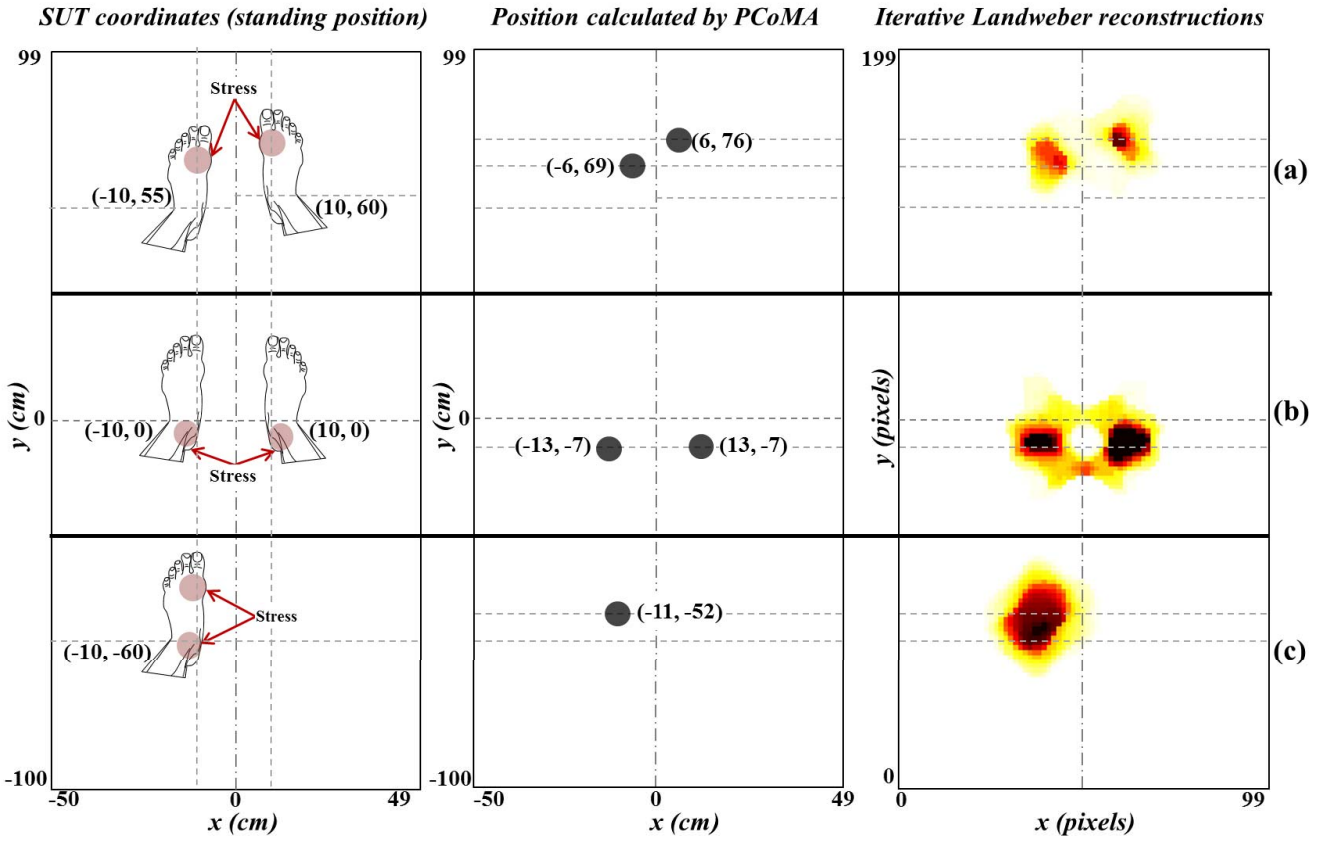

Fig. 8. Three different bare feet positions in rows (a), (b) and (c) of SUT (left column), with the coordinates of the calcaneus bone shown, along with results from PCoMA calculations (center column) and ILM image reconstruction (right column): (a) the weight is on the metatarsus bones; (b) the weight is on the calcaneus bones; and (c) the weight is balanced on the left foot.

carpet" based on PGPT, the output of such algorithms should be interpreted as "Center of Deformation".

The following section presents results obtained by ILM with median filtering, as well as by the PCoMA. These algorithms were either run in real time on acquired and processed data, or applied on previously acquired datasets, as indicated below.

D. System Performance Example

The system performance was tested by routine standing and walking on the sensor head. Fig. 7(a) and Fig. 7(b) show snapshots, taken with shoes, of two typical feet positions: (a) standing and (b) walking. The left panels show photographic images for reference, while the right panels show the ILM reconstructions. The full reconstruction grid was 80 pixels $\times$ 160 pixels; however, for display purposes the figures are cropped to 70 $\times$ 90 pixels to retain only sections with significant data. The reconstructions imply that stepping on the heels and the front of the sole can be distinguished in the footprint. This is explained by the specific shape of the sole, resulting in larger deformation of the underlay just beneath these locations. A real-time reconstructed frame sequence can be watched by downloading the multimedia file accessible from IEEE*Xplore*®. A balanced posture with bare feet shown in Fig. 7(c) allows clearer distinction of the deformation under the metatarsal and calcaneus bones, as expected since the sensor was designed to allow spatial resolution of 0.06 m (taken as the distance between adjacent path integrals).

The PCoMA and ILM performance were studied off-line, on special datasets obtained from the sensor head with a view to attempting a numerical comparison between the actual and calculated spatial positions. The results obtained with bare feet are displayed in Fig. 8, on a 200 pixel $\times$ 100 pixel grid, common for the actual position, PCoMA and ILM reconstruction displays (left, center and right panels, respectively, with x = 0 cm and pixel number 50 shown as a dash-dotted line). The pixel grid accurately corresponds to the real dimensions of the carpet in cm.

The first two rows in Fig. 8 show two different cases of standing on both legs: (a) weight on the metatarsal bones (ball of the foot) and (b) on the calcaneus bones (heel), respectively. Row (c) is a case of standing on one leg. The actual position of the feet in any of the three cases (a), (b) and (c) is defined by the projection onto the ground of the medial malleolus position. These coordinates are shown as the crossings of dashed lines in the left panel. The horizontal dashed lines are replicated in the middle and right panels to visualize the shift of the centers of deformation in the middle panel (PCoMA) and the changes in the reconstructed images in the right panel (ILM). The coordinates of all five foot positions are shown in the left panel. These coordinates were marked in advance as locations on the surface of the carpet and the

measurements were taken by aligning the medial malleolus with these locations, as required for cases (a), (b) and (c), to the best of the subject's ability.

VI. Discussion and Conclusion

In case (a), Fig. 8, it is possible to observe the effect of the comparatively larger contact area when the metatarsus and possibly the toes (hallux) are involved - the deformation is weaker and the region imaged by ILM is more compact than in (b) and (c). The relative positions of the two feet are reproduced correctly: in (a) there is a common shift of $\sim$15 cm towards the front of both feet. This is in clear distinction from case (b) resulting from standing on the heels. Here the exerted pressure is larger, due to the shape of the calcaneus bone, and the deformation region is spread further. Compared to the actual feet coordinates, the calculated CoM coordinates show for both feet a clear displacement of as much as 7 cm towards the back of the feet and about 3 cm outwards. In case (c), in order to keep the balance, stress is naturally distributed on both, metatarsal and calcaneus bones. Furthermore, the pressure is doubled, resulting in stronger deformation affecting areas spread further, as observed by ILM. The center of deformation is shifted with about 8 cm towards the front of the foot, which corroborates that the pressure is more evenly distributed between the heel and the ball of the foot, compared to the other cases. There is generally good consistency in the PCoMA calculations and the ILM reconstructions.

In summary, we report on a complete "intelligent carpet" system based on POF sensors, which is capable of real-time imaging of human footprint by means of PGPT. The imaging contrast is defined as the deformation of the underlay resulting from stepping on the carpet pile. The "intelligent carpet" can be built into new living environments or retro-fitted without major disruptions. It does not introduce new objects in the household and does not require any special attention or action outside the routine. The intrusion in privacy can be reduced to negligible, as the system can be set to communicate externally only the agreed and necessary level of detail.

In healthcare alone, further progress will be inspired by the indicated capability to distinguish between the calcaneus and metatarsus bones, as suggested by Fig. 8. Given that the existing hardware can drive the electronics (LEDs sequences and acquisition) at frame data rates of up to 60 Hz and the fast PCoMA algorithm, we already exceed the 10 FPS threshold required for analysis of walking patterns. For real-time imaging the speed was capped at 3 FPS because of the particular external inexpensive hardware, which can be upgraded or replaced with hardware acceleration.

The intelligent carpet technology can be integrated with other POF sensing techniques to provide a more holistic picture of patterns of activity and rest. Changes in activity levels, gait or balance are indicators of health deterioration often leading to adverse events such as a fall or hospitalization, affecting a high proportion of the population. Remote data collection and wireless connectivity to the community and relevant care services can be achieved seamlessly by customizing the intelligent front-end of the system. It is conceivable that the "intelligent carpet" can be deployed on its own or as a baseline sensing platform for fusion with other sensors to analyze change in behavior and gait. This could provide health care professionals with forewarning of deterioration, enabling early intervention with concomitant cost savings, to both healthcare and the individual, by reducing adverse events.

The application spectrum of the demonstrated technology is vast and it is not our goal to address it here. Obvious domains, outside the healthcare sector, such as sports, security and the manufacturing industry can be served, possibly with modifications of the POF bending sensitivity.

References

[1] R. Assente, G. Ferigno, and A. Pedotti, "Distributed multiplexing architecture for PVDF multitransducer platform scanning: A theoretical and practical approach," in *Proc. 5th Syrup. Electrets*, Heidelberg, Germany, 1985, pp. 795–800.

[2] J. Paradiso, C. Abler, K.-Y. Hsiao, and M. Reynolds, "The magic carpet: Physical sensing for immersive environments," *CHI Late-Breaking/Short Demonstration*, 1997, pp. 277–278.

[3] L. Middleton, A. A. Buss, A. Bazin, and M. S. Nixon, "A floor sensor system for gait recognition," in *Proc. 4th IEEE Workshop Autom. Identificat. Adv. Technol. (AutoID)*, Oct. 2005, pp. 171–176.

[4] M. D. Addlesee, A. Jones, F. Livesey, and F. Samaria, "The ORL active floor [sensor system]," *IEEE Pers. Commun.*, vol. 4, no. 5, pp. 35–41, Oct. 1997.

[5] S. Rangarajan, A. Kidane, G. Qian, S. Rajko, and D. Birchfield, *The Design of a Pressure Sensing Floor for Movement Based Human Computer Interaction*. Berlin, Germany: Springer-Verlag, 2007.

[6] D. Savio and T. Ludwig, "Smart carpet: A footstep tracking interface," in *Proc. 21st Int. Conf. Adv. Inf. Netw. Appl. Workshops (AINAW)*, May 2007, pp. 754–760.

[7] S. Schumer, "Analysis of human footsteps utilizing multi-axial seismic fusion," in *Proc. IEEE Int. ICASSP*, May 2011, pp. 697–700.

[8] Y. Guo and M. Hazas, "Localising speech, footsteps and other sounds using resource-constrained devices," in *Proc. 10th Int. Conf. Inf. Process. Sensor Netw. (IPSN)*, Apr. 2011, pp. 330–341.

[9] R. J. Orr and G. D. Abowd, "The smart floor: A mechanism for natural user identification and tracking," in *CHI Short Talks*, 2000, pp. 275–276.

[10] K. Nakajima, Y. Mizukami, K. Tanaka, and T. Tamura, "Footprint-based personal recognition," *IEEE Trans. Biomed. Eng.*, LNCS 47, no. 11, pp. 1534–1537, Nov. 2000.

[11] J. Suutala, K. Fujinami, and J. Röning, "Gaussian process person identifier based on simple floor sensors," in *Proc. 3rd EuroSSC*, vol. 5279. 2008, pp. 55–68.

[12] J. Suutula and J. Röning, "Methods for person identification on a pressure-sensitive floor: Experiments with multiple classifiers and reject option," *Inf. Fusion*, vol. 9, no. 1, pp. 21–40, 2008.

[13] Y.-L. Shen and C.-S. Shin, "Distributed sensing floor for an intelligent environment," *IEEE Sensors J.*, vol. 9, no. 12, pp. 1673–1678, Dec. 2009.

[14] A. Uhl and P. Wild, "Footprint based biometric verification," *J. Electron. Imag.*, vol. 17, no. 1, pp. 011016-1–011016-10, 2008.

[15] L. Wen-Hau, C.-L. Wu, and L.-C. Fu, "Inhabitants tracking system in a cluttered home environment via floor load sensors," *IEEE Trans. Autom. Sci. Eng.*, vol. 5, no. 1, pp. 10–20, Jan. 2008.

[16] D. Gafurov and E. Snekkenes, "Gait recognition using wearable motion recording sensors," *EURASIP J. Adv. Signal Process.*, vol. 2009, p. 415817, Jun. 2009.

[17] C. Hodt-Billington, J. L. Helbostad, and R. Moe-Nilssen, "Should trunk movement or footfall parameters quantify gait asymmetry in chronic stroke patients?" *Gait Posture*, vol. 27, no. 4 pp. 552–558,A real-time reconstructed framesequence can be watched by downloadingthe multimedia file accessible from IEEE Xplore. A balanced posture with bare feet shown in Fig. 7(c) allows clearer distinction 2008.

[18] K. B. Ozanyan, S. G. Castillo, and F. J. P. Ortiz, "Guided-path tomography sensors for nonplanar mapping," *IEEE Sensors J.*, vol. 5, no. 2, pp. 167–174, Apr. 2005.

[19] A. R. Niemeijer, B. J. M. Frederiks, I. I. Riphagen, J. Legemaate, J. A. Eefsting, and C. M. P. M. Hertogh, "Ethical and practical concerns of surveillance technologies in residential care for people with dementia or intellectual disabilities: An overview of the literature," *Int. Psychogeriatrics*, vol. 22, no. 7, pp. 1129–1142, 2010.

[20] N. Nurgiyatna, P. Scully, and K. B. Ozanyan, "Grooved fiber sensors for deformation imaging," in *Proc. IEEE Sensors Conf.*, Nov. 2010, pp. 1675–1678.

[21] J. A. Cantoral-Ceballos, N. Nurgiyatna, P. Scully, and K. B. Ozanyan, "Smart carpet for imaging of objects' footprint by photonic guided-path tomography," in *Proc. IEEE AFRICON*, Livingstone, Zambia, Sep. 2011, pp. 1–6.

[22] N. Fang, L. Wang, D. Jia, and C. Shan, and Z. Huang, "Walking intrusion signal recognition method for fiber fence system," in *Proc. Asia Commun. Photon. Conf. Exhibit. (ACP)*, Nov. 2009, pp. 1–6.

[23] C. L. Saltzman, D. A. Nawoczenski, and K. D. Talbot, "Measurement of the medial longitudinal arch," *Archives Phys. Med. Rehabil.*, vol. 76, no. 1, pp. 45–49, 1995.

[24] R. V. Rodríguez, R. P. Lewis, J. S. D. Madison, and N. W. D Evans, "Footstep recognition for a smart home environment," *Int. J. Smart Home*, vol.2, no. 2, pp. 95–110, Apr. 2008.

[25] R. Vera-Rodriguez, R. P. Lewis, J. S. D. Madison, and N. W. D. Evans, "A large scale footstep database for biometric studies created using cross-biometric for labelling," in *Proc. 10th ICARV*, Dec. 2008, pp. 1361–1366.

[26] (2012). *GAITRite Electronic Walkway Technical Reference*. [Online]. Available: http://www.gaitrite.com/Downloads/GAITRite_Measurement_Definitions.pdf

[27] G. F. Fernando, "Fibre optic sensor systems for monitoring composite structures," *Reinforced Plastic*, vol. 49, no. 11, pp. 41–49, 2005.

[28] R. Philip-Chandy, P. J. Scully, and R. Morgan, "The design, development and performance characteristics of a fibre optic drag-force flow sensor," *Meas. Sci. Technol.*, vol. 11, no. 3, pp. N31–N35, 2000.

[29] K. S. C. Kuang, W. J. Cantwell, and P. J. Scully, "An evaluation of a novel plastic optical fibre sensor for axial strain and bend measurements," *Meas. Sci. Technol.*, vol. 13, no. 10, pp. 1523–1534, 2002.

[30] L. Renqiang, F. Zhuang, Z. Yanzheng, C. Qixin, and W. Shuguo, "Operation principle of a bend enhanced curvature optical fiber sensor," in *Proc. IEEE/RSJ Int. Conf. Intell. Robots Syst.*, Beijing, China, Oct. 2006, pp. 1966–1971.

[31] D. Z. Stupar, J. S. Bajic, L. M. Manojlovic, M. P. Slankamenac, A. V. Joza, and M. B. Zivanov, "Wearable low-cost system for human joint movements monitoring based on fiber-optic curvature sensor," *IEEE Sensors J.*, vol. 12, no. 12, pp. 3242–3431, Dec. 2012.

[32] L. Bilro, J. G. Oliveira, J. L. Pinto, and R. N. Nogueira, "A reliable low-cost wireless and wearable gait monitoring system based on a plastic optical fibre sensor," *Meas. Sci. Technol.*, vol. 22, no. 4, pp. 045801-1–045801-7, 2011.

[33] M. Donno, E. Palange, F. D. Nicola, G. Bucci, and F. Ciancetta, "A new flexible optical fiber goniometer for dynamic angular measurements: Application to human joint movement monitoring," *IEEE Trans. Instrum. Meas.*, vol. 57, no. 8, pp. 1614–1620, Aug. 2008.

[34] A. Babchenko and J. Maryles, "A sensing element based on 3D imperfected polymer optical fibre," *J. Opt. A, Pure Appl. Opt.*, vol. 9, no. 1, pp. 1–5, Jan. 2007.

[35] Y. Fu and H. Di, "Fiber-optic curvature sensor with optimized sensitive zone," *Opt. Laser Technol.*, vol. 43, no. 3, pp. 586–591, Apr. 2011.

[36] Y. Fu, H. Di, and R. Liu, "Light intensity modulation fiber-optic sensor for curvature measurement," *Opt. Laser Technol.*, vol. 42, no. 4, pp. 594–599, Jun. 2010.

[37] M. S. Kovacevic, A. Djordjevich, and D. Nikezic, "Analytical optimization of optical fiber curvature gauges," *IEEE Sensors J.*, vol. 8, no. 3, pp. 227–232, Mar. 2008.

[38] T. York, H. McCann, and K. B. Ozanyan, "Agile sensing systems for tomography," *IEEE Sensors J.*, vol. 11, no. 12, pp. 3086–3105, Dec. 2011.

[39] K. B. Ozanyan, N. Nurgiyatna, E. P. A. Constantino, J. Vaughan, and P. Scully, "Photonic guided-path tomography sensor for deformation in a non-planar surface," *J. Phys., Conf. Ser.*, vol. 178, no. 1, p. 012025, 2009.

[40] A. C. Kak and M. Slaney, *Principles of Computerized Tomographic Imaging*. New York, NY, USA: IEEE Press, 1988.

[41] S. Joshua, Y. M. Keung, P. J. Scully, and K. Ozanyan, "Photonic guided-path tomography for imaging pressure distribution using polymer optical fibre strain sensors," in *Proc. 18th Int. Conf. Opt. Fiber Sensors*, Cancun, Mexico, Oct. 2006, pp. 1–4.

[42] N. Nurgiyatna, J. Davidson, K. B. Ozanyan, J. Vaughan, and P. Scully, "Photonic guided-path tomography with fibre transducers," in *Proc. 5th World Congr. Ind. Process Tomogr.*, Bergen, Norway, 2007, pp. 149–155.

[43] T.-S. Pan and A. E. Yagle, "Acceleration of Landweber-type algorithms by suppression of projection on the maximum singular vector," *IEEE Trans. Med Imag.*, vol. 11, no. 4, pp. 479–487, Dec. 1992.

[44] W. Q. Yang, D. M. Spink, T. A. York, and H. McCann, "An image-reconstruction algorithm based on Landweber's iteration method for electrical-capacitance tomography," *Meas. Sci. Technol.*, vol. 10, no. 11, pp. 1065–1069, 1999.

[45] N. Terzija *et al.*, "Image optimization for chemical species tomography with an irregular and sparse beam array," *Meas. Sci. Technol.*, vol. 19, no. 9, pp. 094007–094019, 2008.

[46] E. P. A. Constantino and K. B. Ozanyan, "Tomographic imaging of surface deformation from scarce measurements via sinogram recovery," *IEEE Sensors J.*, vol. 9, no. 4, pp. 399–410, Apr. 2009.

[47] J. Cantoral-Ceballos and K. Ozanyan, "Parallel-data reconstruction for limited views tomography sensors by sinusoidal Hough transform," *IEEE Sensors J.*, vol. 13, no. 2, pp. 581–588, Feb. 2013.

[48] E. P. A. Constantino and K. B. Ozanyan, "Sinogram recovery for sparse angle tomography using a sinusoidal Hough transform," *Meas. Sci. Technol.*, vol. 19, no. 9, p. 094015, 2008.

Jose A. Cantoral-Ceballos (S'10–M'14) received the B.Sc. (Hons.) degree in electronic and communications engineering from the Instituto Tecnológico y de Estudios Superiores de Monterrey, Queretaro, Mexico, in 2005, and the M.Sc. (Distinction) and Ph.D. degrees from the University of Manchester, Manchester, U.K., in 2009 and 2013, respectively, with a focus on tomography imaging from limited data.

He was a Project Engineer with CIATEQ A.C., Mexico, from 2005 to 2008, where he was involved in the development of supervisory control and data acquisition systems for the oil and gas industry. He is currently a Post-Doctoral Research Associate with the University of Manchester.

Dr. Cantoral-Ceballos was a recipient of the National Instruments Prize for his M.Sc. dissertation in 2009 and the Best Technical Presentation Award at the Seventh WCIPT, Krakow, in 2013.

Nurgiyatna Nurgiyatna received the B.Sc. degree in electrical engineering from the Universitas Gadjah Mada, Indonesia, in 1999, and the M.Sc. and Ph.D. degrees from the University of Manchester, Manchester, U.K., in 2006 and 2013, respectively, with a focus on imaging systems based on plastic optical fibers. He was a recipient of the National Instruments Prize for his M.Sc. Dissertation in 2006.

He was a Lecturer with the Department of Electrical, Electronic and Informatics Engineering, Universitas Muhammadiyah Surakarta (UMS), Indonesia, from 2000 to 2008. He is currently with UMS.

Paul Wright received the B.Sc. (Hons.) degree in pure and applied physics from the University of Nottingham, Nottingham, U.K., in 1993, and the Ph.D. degree in physics from the University of Exeter, Exeter, U.K., in 1997.

He was a Lecturer with the Division of Measurement and Control, University of Teesside, before spending five years with Land Infrared, as a Project Engineer working on industrial applications of optical thermometry. He joined the University of Manchester, Manchester, U.K., in 2002, where he is currently a Lecturer. Throughout his career, he has designed numerous optical and electronic instruments and has co-authored publications on near-IR thermometry, optical tomography, and medical instrumentation. He is the recipient of the Maurice Beck Prize for the Best Paper at the Fifth WCIPT (Bergen, 2007) and the Best Poster at Photon 06 (Manchester, 2006).

John Vaughan received the B.Sc. (Hons.) degree in ecology from the University of East Anglia, Norwich, U.K., and the M.Sc. degree in instrumentation and analytical science and the Ph.D. degree in optoelectronic environmental sensors and surface enhanced Raman spectroscopy from the University of Manchester Institute of Science and Technology, Manchester, U.K., in 2001 and 2004, respectively. He was a Knowledge Transfer Research Associate with Unilever and the University of Manchester, Manchester, in *in vivo* polymer sensors for perspiration monitoring and in a EU-funded project installation permitting guidance for hydrogen and fuel cells stationary applications. His research interests include optical fiber sensors, laser technology, and optical sensing and measurement.

Christine Brown-Wilson was a registered Nurse in Sydney, Australia, in 1981, and received the B.Sc. (Hons.) degree in nursing from Christ Church University College, Canterbury, U.K., in 1999, and the Ph.D. degree in nursing from the University of Sheffield, Sheffield, U.K., in 2007. She worked with older people in a range of health care environments holding academic positions with the University of Sheffield (2002–2007), and is currently the Program Director at the University of Manchester, Manchester, U.K. Her research interests include cognitive and physical frailty in older people living in supported and community environments. She has authored a book on *Caring for Older People* (London, U.K.: Sage, 2012), and is involved in research in the this field in the U.K. and Singapore. She is a Fellow of the Higher Education Academy and a Member of the Royal College of Nursing.

Patricia J. Scully received the B.Sc. (Hons.) degree in physics from the University of Manchester, Manchester, U.K., in 1985, the M.Sc. degree in instrumentation and analytical science from the University of Manchester Institute of Science and Technology, Manchester, in 1986, and the Ph.D. degree in engineering from the University of Liverpool, Liverpool, U.K., in 1992. She was a Lecturer, Senior Lecturer, and Reader with Liverpool John Moores University, Liverpool, from 1990 to 2002, and is currently a Senior Lecturer in Sensor Instrumentation with the University of Manchester. Her research interests include photonic sensors and optical instrumentation, femtosecond laser writing of photonic structures, chemically sensitive optical coatings for polymers, optical sensing and measurement, optical fiber sensors, polymer optical fibers, and optical fiber technology. She is a Senior Academic/Associate Professor with experience in leading industrial and research council/government funded research projects at national and international levels.

Krikor B. Ozanyan (M'95–SM'03) received the M.Sc. degree in engineering physics (semiconductors) and the Ph.D. degree in solid-state physics from the University of Sofia, Sofia, Bulgaria, in 1980 and 1989, respectively.

He has held previous academic and research positions with the University of Sofia, the Norwegian Institute of Technology, Trondheim, Norway, the University of Hull, Hull, U.K., and the University of Sheffield, Sheffield, U.K., working on projects ranging from Brewster-angle mid-IR spectroscopic ellipsometry and electron confinement in quantum wells and barriers, to the demonstration of the lasing at 333 nm from strained MQW ZnCdS/ZnS structures and *in situ* real-time optical monitoring of growth of III–V semiconductors in MBE and MOCVD reactors. His current interests are in the area of photonic sensors and indirect imaging (tomography) by optical modalities, signal processing for optical experiments, and spectroscopy with ultrafast laser sources. He is currently Head of Sensors, Imaging, and Signal Processing at the University of Manchester, Manchester, U.K., and a Visiting Professor at the University of Bergen, Bergen, Norway.

Prof. Ozanyan is a Fellow of the Institute of Engineering and Technology, U.K, and the Institute of Physics, U.K. He was a Distinguished Lecturer of the IEEE Sensors Council from 2009 to 2010, and the Guest Editor of the IEEE SENSORS JOURNAL Special Issues on "Sensors for Industrial Process Tomography" in 2005 and "THz Sensing: Materials, Devices and Systems" in 2012. He is currently the Editor-in-Chief of the IEEE SENSORS JOURNAL.